# Photoproduction and electroproduction of $\Lambda(1405)$ via $\gamma^{(*)}p \to K^{*+}\pi^0\Sigma^0$

Seung-il Nam[1,2,3,*] and Atsushi Hosaka[4,5,†]

[1]*Department of Physics, Pukyong National University (PKNU), Busan 48513, Korea*
[2]*Center for Extreme Nuclear Matters (CENuM), Korea University, Seoul 02841, Korea*
[3]*Asia Pacific Center for Theoretical Physics (APCTP), Pohang 37673, Korea*
[4]*Research Center for Nuclear Physics (RCNP), Ibaraki, Osaka 567-0047, Japan*
[5]*Advanced Science Research Center, Japan Atomic Energy Agency (JAEA), Tokai 319-1195, Japan*

(Received 10 March 2019; revised manuscript received 10 May 2019; published 23 July 2019)

We study the photoproduction and electroproductions of the vector kaon off the proton, i.e., $\gamma^{(*)}p \to K^{*+}\pi^0\Sigma^0$, and investigate the line shape of the $\pi^0\Sigma^0$ invariant mass in an effective Lagrangian approach with the inclusion of a $K^*N\Lambda^*$ interaction. Relevant electromagnetic form factors for the neutral hyperons and charged strange mesons are constructed by considering experimental and theoretical information. We find that the $\Lambda^*$ peak is clearly observed for the photoproduction and electroproductions with the finite $K^*N\Lambda^*$ interaction, whereas the clear peak signals survive only for the electroproduction, when we ignore the interaction. These different behaviors can be understood by different $Q^2$ dependencies in the $K^*$ electromagnetic and $K^* \to \gamma K$ transition form factors. We suggest a photon-polarization asymmetry $\Sigma$ to extract information of the $K^*N\Lambda^*$ interaction. It turns out that $\Sigma$ near the $\Lambda^*$ peak region becomes negative with a finite $K^*N\Lambda^*$ interaction while positive without it for $Q^2 = 0$, because of the different naturalities of $K$ and $K^*$ exchanges. For $Q^2 \neq 0$, we observe more obvious signals in the peak region owing to the additional contribution of the longitudinal virtual photon for $\Lambda^*$.

DOI: 10.1103/PhysRevC.100.015205

## I. INTRODUCTION

Hadron spectroscopy is one of the most active fields to understand the nature of the low-energy (nonperturbative) strong interactions of quarks and gluons, being governed by quantum chromodynamics (QCD). In the low-energy region, it is believed that chiral symmetry plays an important role, which provides nontrivial mechanisms to generate the masses of hadrons as known by spontaneous breakdown of chiral symmetry (SBCS). Based on this idea, effective field theories have been developed in terms of the chiral dynamics with the pseudoscalar (PS) meson degrees of freedom because the PS mesons are the massless-mode realization of SBCS, i.e., chiral perturbation theory (ChPT) [1]. Beyond perturbation, $p$-wave baryon resonances of negative parity have been explored with the help of a unitarity condition in the coupled-channel approach [2–5] with much success.

It is worth mentioning that the chiral unitary model (ChUM) is a very useful theoretical tool to address low-lying $s$-wave baryon resonances [5]. Among successful descriptions of the resonances, the model suggests that $\Lambda(1405, 1/2^-) \equiv \Lambda^*$ is a meson-baryon molecular state rather than a simple three-quark one. Moreover, the line shape of the production data via $\gamma p \to K^+\pi\Sigma$ can be interpreted by the *destructive* interference of the two poles in the complex energy plane [6], where the higher-mass pole at $(1430 + 15i)$ MeV couples strongly to the $\bar{K}N$ channel and the lower-mass pole at $(1376 + 63i)$ MeV to the $\pi\Sigma$ one by analyzing the residues of the PS-meson-baryon scattering amplitudes in ChUM. Basically, the two poles appear in the second Riemann sheet as resonances through the attractive $S = -1$ chiral interactions in the coupled-channel amplitudes [5].

The pole positions were extensively investigated theoretically fitting the experimental data via ChUM [7,8]. The two-pole scenario was supported in various theoretical approaches, including the recent lattice-QCD simulation for its strange magnetic form factor [9] and the detailed analysis for the low-energy $\bar{K}N$ amplitude [10]. Recently, the CLAS (CEBAF Large Acceptance Spectrometer) collaboration at Jefferson laboratory (JLab) reported in Ref. [11] that the invariant-mass line shape from the electroproduction of kaon in $\gamma^* p \to K^+\pi\Sigma$ shows two bump structures in the vicinity of $M_{\pi\Sigma} = (1.35 \sim 1.45)$ GeV which is quite different from that of photoproduction data [12–14]. In our previous work [6], this distinctive feature of the invariant-mass line shape was explained by the different interference pattern from the electromagnetic (EM) form factors of the two poles: The interference between the two poles becomes *constructive*, resulting in the two bumps appearing near the higher and lower pole positions. Although there were some theoretical

*sinam@pknu.ac.kr
†hosaka@rcnp.osaka-u.ac.jp

uncertainties, this observation supports the two-pole scenario for the $\Lambda^*$ structure [15].

In the present work, we would like to investigate the interference effects of the two poles and the invariant-mass line shapes carefully, in a different production-reaction process with the vector kaon ($K^*$), i.e., $\gamma^{(*)}p \to K^{*+}\pi^0\Sigma^0$. Because there are so far only a limited experimental data for $K^*$ productions, many of our results shown here are predictions and provide a guideline for the future experiments. This reaction process can be performed experimentally by the LEPS (Laser Electron Photon beam-line at SPring-8) at SPring-8 (Super Photon Ring - 8 GeV) and CLAS collaborations in the future. Because this reaction process does not contain the $\Sigma^*(1385)$ contribution, one is free from the interference between $\Sigma^*$ and $\Lambda^*$, resulting in a clear signal only from $\Lambda^*$ in the vicinity of the invariant mass $M_{\pi^0\Sigma^0} = (1.35 \sim 1.45)$ GeV. In addition to focusing on the differences between the photoproduction and electroproductions of $\Lambda^*$, one of the theoretical motivations of the present work is to estimate the strong-coupling strength of $g_{K^*N\Lambda^*}$, which is rarely studied in theories and experiments. For instance, in Ref. [16], $g_{K^*N\Lambda^*}$ was estimated using the ChUM approach with the Kroll-Ruddermann (KR) interaction in terms of the vector dominance. Taking the present situation into consideration, we also want to provide a unique experimental method to determine the $K^*N\Lambda^*$ interaction strength by taking into account the incident-photon polarizations. The study of vector mesons provides information on their dynamics which is as important as of the Nambu-Goldstone bosons.

As a theoretical tool to study the present reaction process, we employ the effective Lagrangian method at the tree-level Born approximation together with the theoretical and experimental inputs for the strong and electromagnetic (EM) hadron properties. As for the strong form factors, we make use of the conventional Lorentzian type as done in our previous works [6,17], whereas the neutral-hyperon EM form factors are parametrized by using the information of their electric charge radii, which were computed by various theoretical models including ChUM [15,18]. The theoretical results of Ref. [19] are used to parametrize the EM form factor of the charged vector kaon, and the $K^* \to \gamma K$ transition form factor is devised by combining the light-cone sum rule [20] and the kaon light-cone wave function, which was computed using the nonlocal chiral-quark model based on the instanton QCD vacuum by the authors [21,22]. The gauge-invariant prescription is also taken into account to satisfy the Ward-Takahashi (WT) identity for both of the photoproduction and electroproductions [6].

As for the invariant-mass line shape $d\sigma/dM_{\pi^0\Sigma^0}$, we find that the lower-pole contribution of $\Lambda^*$ turns out to be much smaller than the higher one, when results of ChUM results are employed in reaction calculations. Therefore, we do not have considerable interferences between the two poles for $\Lambda^*$ in the present reaction process. The background (BKG) contribution comes mainly from the destructive and constructive interferences between $\Lambda$ and $\Sigma$ ground-state contributions for the photoproduction and electroproductions, respectively, because their EM form factors change the relative signs between the invariant amplitudes. We also find that the $\Lambda^*$ peak is clearly observed for the photoproduction and electroproductions with the finite $K^*N\Lambda^*$ interaction, whereas the peak survives only for the photoproduction when we ignore the interaction. These behaviors of the peak can be finally understood by the different $Q^2$ dependencies in the $K^*$ electromagnetic and $K^* \to \gamma K$ transition form factors. Finally, we suggest a photon-polarization observable $\Sigma$, which identifies the strength of the $K^*N\Lambda^*$ interaction uniquely. It turns out that the value of $\Sigma$ near the $\Lambda^*$ peak region $M_{\pi^0\Sigma^0} = 1.43$ GeV becomes negative with the interaction and positive without it for $Q^2 = 0$, according to the different interaction structure of $K$ and $K^*$ with respect to the polarized photon. As for $Q^2 \neq 0$, we observe similar but clearer signals, but the $\Sigma$ curves slightly change, because the scalar component of the photon polarization enhances the spin-1 exchange.

The present paper is organized as follows: In Sec. II, we briefly introduce the theoretical framework. The numerical results and relevant discussions are given in Sec. III, and Sec. IV is devoted to the summary of the present work.

## II. THEORETICAL FRAMEWORK

In this section, we would like to describe the theoretical framework briefly, based on the effective Lagrangian approach in the tree-level Born approximation. The relevant Feynman diagrams for $\gamma^{(*)}p \to K^{*+}\pi\Sigma$ are shown in Fig. 1, in which we also define the four momenta for each particle involved. Namely, the momenta $k_{1\sim5}$ are for the particles participating in the reaction as shown in Fig. 1. Figures 1(a) and 1(c) are responsible in that the amplitude satisfies the Ward-Takahashi identity (WTI) for the pseudoscalar (PS) $PBB$ coupling scheme, where $P$ and $B$ indicate the PS meson and spin-1/2 baryon, respectively. Note that Fig. 1(b) is gauge invariant by itself, owing to its magnetic photon-coupling structure. Figure 1(d) denotes the PS kaon exchange. As for the diagrams, where hyperons $Y^{(*)}$ appear as intermediate states, we consider $\Lambda(1116, 1/2^+)$, $\Sigma^0(1192, 1/2^+)$, $H(1430, 1/2^-)$, and $L(1390, 1/2^-)$, in which $H$ and $L$ indicate the higher- and lower-pole contributions for $\Lambda(1405, 1/2^-)$, respectively.

Note that $\Sigma^{*0}(1385)$ is not taken into account here because it does not couple to the neutral $\pi^0\Sigma^0$ channel, owing to the vanishing isospin Clebsch-Gordan coefficient. However, we can consider the EM transition of $\Lambda$-$\Sigma^{*0}(1385)$, which can be shown in Fig. 1(b) with the $\pi^0\Sigma^0\Lambda$ interaction vertex. However, it turns out that the u-channel amplitude [Fig. 1(b)] is suppressed when the empirical values for the magnetic moments are employed, $\mu_{\Sigma^{*0}\to\gamma\Lambda} = (2.75 \pm 0.25)\,\mu_N$ [23] and $2.28\,\mu_N$ [24], as compared to the others because of the form factor. Therefore, we do not take into account that contribution in the following discussions.

In addition, there can be the contributions from nucleon resonances with $M_{N^*} \approx 2$ GeV in Fig. 1(a) by interchanging $\pi^0$ and $K^{*+}$ for instance [25]. In general, the $N^*$ contributions will appear as sloped bands in the Dalitz plot as a function of $M^2_{K^{*+}\pi^0}$ and $M^2_{\pi^0\Sigma^0}$, and interfere with the hyperon resonances,

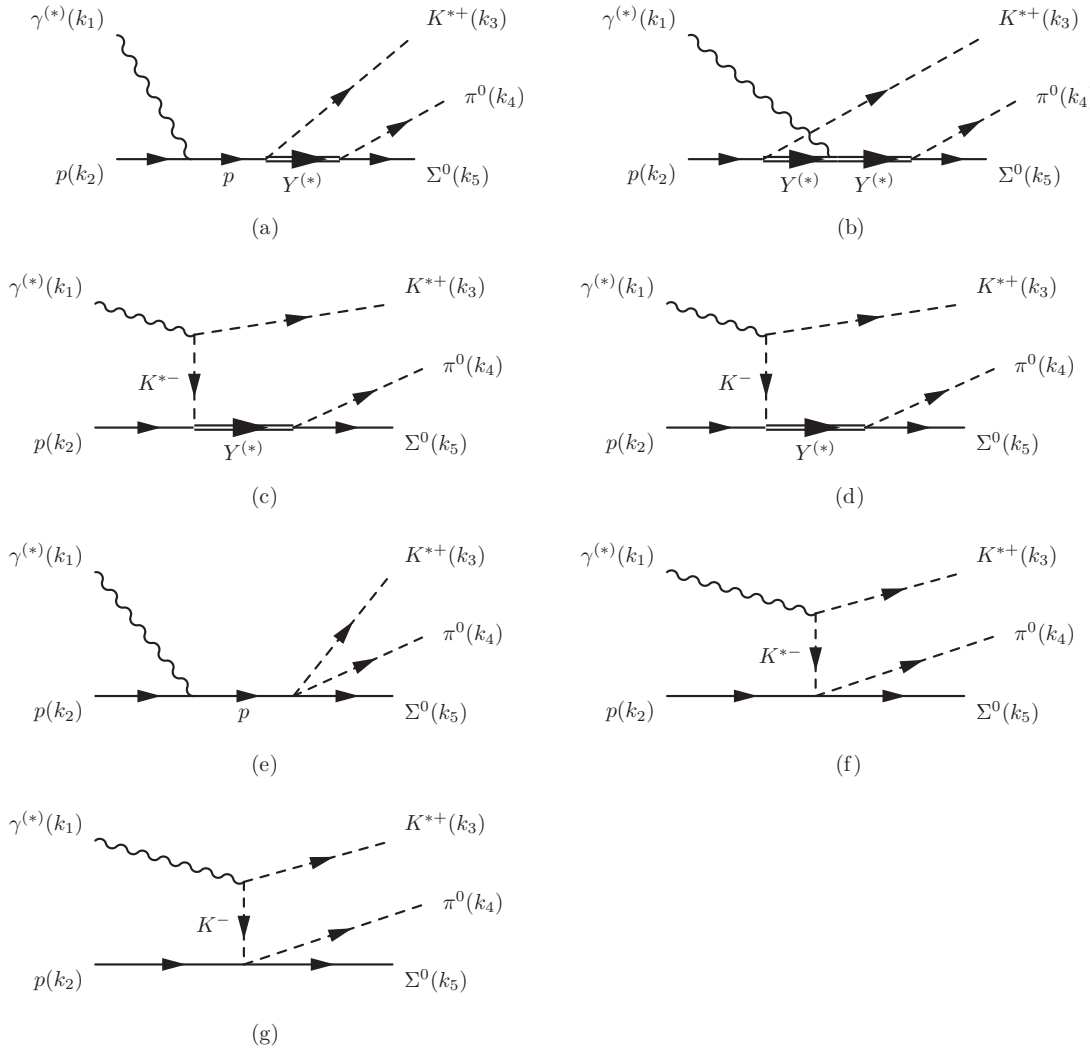


FIG. 1. Relevant Feynman diagrams for $\gamma p \to K^{*+}\pi^0\Sigma^0$: (a) proton-pole diagram in the $s$ channel, (b) hyperon ground-state and resonance diagram in the $u$ channel, (c) $K^*$ exchange in the $t$ channel, (d) $K$ exchange in the $t$ channel, (e) and (f) background contributions from the $PB \to VB$ Kroll-Ruddermann (KR) interaction, and (g) those from the $PB \to PB$ Weinberg-Tomozawa (WT) interaction. As for the hyperons $Y^{(*)}$, we consider $\Lambda(1116, 1/2^+)$, $\Sigma^0(1192, 1/2^+)$, $H(1430, 1/2^-)$, and $L(1390, 1/2^-)$, in which $H$ and $L$ indicate the higher- and lower-pole contributions for $\Lambda(1405, 1/2^-)$, respectively. See the text for details.

such as $\Lambda(1405)$. As observed in the $\gamma p \to K^+K^-p$ reaction process [26], such interference effects are not significant and become negligible, when the decay width of the resonance is considerably wide. Moreover, the coupling constants for $K^*N^*\Sigma$ are rarely determined experimentally, resulting in the increase of theoretical uncertainties. Hence, we do not consider the $N^*$ contributions in the present work somewhat safely.

The diagrams are derived from the Kroll-Ruderman (KR) $VB \to PB$ ($e$ and $f$) and Weinberg-Tomozawa (WT) $PB \to PB$ ($g$) interactions [16]. Here, $V$ stands for the vector mesons, such as $K^*(892, 1^-)$. We note that there are more diagrams, in which the photon couples to the outgoing $\Sigma$. We, however, verified that their contributions are much smaller than those from the diagrams shown in Fig. 1. Therefore, we ignore them in the present work.

To compute the diagrams in Fig. 1, we define the effective Lagrangians for the electromagnetic (EM) and strong interaction vertices as follows:

$$
\begin{aligned}
\mathcal{L}_{\gamma BB} &= -\bar{B}\left[e_B \not{A} - \frac{e\kappa_B}{4M_N}(\sigma \cdot F)\right]B \quad \text{for} \\
B &= N, \Lambda, \Sigma, H, L, \\
\mathcal{L}_{\gamma K^*K} &= g_{\gamma KK^*}\varepsilon^{\mu\nu\alpha\beta}(\partial_\mu A_\nu)(\partial_\alpha K^*_\beta)K + \text{h.c.}, \\
\mathcal{L}_{\gamma K^*K^*} &= -ie_{K^*}A^\mu(K^{*\nu}\mathcal{K}^{*\dagger}_{\mu\nu} - \mathcal{K}^*_{\mu\nu}K^{*\dagger\nu}), \\
\mathcal{K}_{\mu\nu} &= \partial_\mu K^*_\nu - \partial_\nu K^*_\mu, \\
\mathcal{L}_{K^*N(H,L)} &= -g^V_{K^*N(H,L)}(\bar{H}, \bar{L})\not{K}^*\gamma_5 N + \text{h.c.}, \\
\mathcal{L}_{\pi\Sigma(H,L)} &= -ig_{\pi\Sigma(H,L)}(\bar{H}, \bar{L})\boldsymbol{\pi} \cdot \boldsymbol{\Sigma} + \text{h.c.}, \\
\mathcal{L}_{KN(H,L)} &= -ig_{KN(H,L)}(\bar{H}, \bar{L})KN + \text{h.c.}, \\
\mathcal{L}_{\text{WT}} &= -ig_{\text{WT}}\bar{\Sigma}(\pi^\dagger \not{\partial} K - K^\dagger \not{\partial}\pi)N + \text{h.c.}, \\
\mathcal{L}_{\text{KR}} &= -iG_{\text{KR}}g_{\text{KR}}\bar{B}\gamma^\mu\gamma_5(P^\dagger K^*_\mu - PK^{*\dagger}_\mu)B + \text{h.c.}.
\end{aligned}
\tag{1}
$$

TABLE I. Relevant coupling constants for the present work. Note $g = g_{KR}$ defined in Ref [16].

| | $g_{KN\Lambda_H}$ | $g_{K^*N\Lambda_H}$ | $g_{\pi\Sigma\Lambda_H}$ | $g_{KN\Lambda_L}$ | $g_{K^*N\Lambda_L}$ | $g_{\pi\Sigma\Lambda_L}$ |
|---|---|---|---|---|---|---|
| $g=0$ | $2.4+1.1i$ | $0.0+i0.0$ | $-0.2-1.4i$ | $1.4-1.6i$ | $0.0+0.0i$ | $-2.3+1.4i$ |
| $g=1$ | $2.4+1.1i$ | $0.1-0.9i$ | $-0.2-1.3i$ | $1.4-1.6i$ | $-0.4+0.1i$ | $-2.3+1.5i$ |

| $g_{KN\Lambda}$ | $g_{K^*N\Lambda}$ | $g_{\pi\Sigma\Lambda}$ | $g_{KN\Sigma}$ | $g_{K^*N\Sigma}$ | $g_{\pi\Sigma\Sigma}$ | $g_{K^*N\Sigma^*}$ | $g_{\pi\Sigma\Sigma^*}$ | $g_{\gamma K^{*+}K^-}$ | $g_{\rm WT}$ | $G_{\rm KR}$ |
|---|---|---|---|---|---|---|---|---|---|---|
| $-13.89$ | $-4.26$ | 11.86 | 4.08 | $-2.46$ | 11.89 | $-2.60$ | 0.55 | $-\frac{0.254}{\rm GeV}$ | $\frac{1}{8f_\pi^2}$ | $\frac{0.34}{4f_\pi}$ |

As for the $\pi\Sigma B$ and $KNB$ interactions we replace $(H, L)$ into $\gamma_5 B$ in the Lagrangians. Because of the lack of experimental and theoretical information, we ignored the tensor coupling $g^T_{K^*N(H,L)}$ throughout this work. The $PBB$ coupling constants corresponding to $H$ and $L$ were estimated by the residues for the higher and lower poles for the $\Lambda(1405)$ in the complex energy plane [5]. In Ref. [16], the values for $g_{K^*N(H,L)}$ and $g_{KN(H,L)}$ were given as functions of the KR coupling $g_{\rm KR} \equiv g = (1 \sim 6)$. Because the values of $g_{K^*N(H,L)}$ are nearly proportional to $g$ [16], we examine the case with $g = 1$ for the most part of the present work. As for the charged transition $\gamma PV$ vertex, we use $g_{\gamma K^{*+}K^+} = 0.254\,{\rm GeV}^{-1}$ [27].

In addition, we will take the $\Lambda(1116, 1/2^+)$ and $\Sigma(1192, 1/2^+)$ contributions for Fig. 1(b) as the hyperon backgrounds (BKG). The strong-coupling constants for $\Lambda$ and $\Sigma$ are employed from the Nijmegen soft-core potential model (NSC97) [28]. We also take the WT and KR contact interactions into account as the BKG contributions. The coupling constants for those contributions are given by $g_{\rm WT} = 1/8f_\pi^2$ and $G_{\rm KR} = (D-F)/2f_\pi$ for the $\pi^0\Sigma^0$ channels with $D - F = 0.34$ and $f_\pi = 93.3\,{\rm MeV}$ [4]. All the values for the relevant couplings are listed in Table I.

The invariant amplitudes, shown in Figs. 1(a)–1(d), for the *resonance* $(H, L)$ contributions are computed from the effective Lagrangians and resulted in

$$
\begin{aligned}
i\mathcal{M}_a^{H,L} &= \frac{g_{H,L}F_cF_{\rm EM}^p\bar{u}_\Sigma(\not{q}_{4+5}+M_{H,L})\not{\epsilon}^*\gamma_5(\not{q}_{1+2}+M_N)\not{\Gamma}_a(Q^2)u_N}{\left[q_{4+5}^2-M_{H,L}^2-iM_{H,L}\Gamma_{H,L}\right]\left[q_{1+2}^2-M_N^2\right]},\\
i\mathcal{M}_b^{H,L} &= \frac{g_{H,L}F_uF_{\rm EM}^{H,L}\bar{u}_\Sigma(\not{q}_{4+5}+M_{H,L})\not{\Gamma}_b(Q^2)(\not{q}_{2-3}+M_{H,L})\not{\epsilon}^*\gamma_5 u_N}{\left[q_{4+5}^2-M_{H,L}^2-iM_{H,L}\Gamma_{H,L}\right]\left[q_{2-3}^2-M_{H,L}^2\right]},\\
i\mathcal{M}_c^{H,L} &= \frac{g_{H,L}F_cF_{\rm EM}^{K^*}\bar{u}_\Sigma(\not{q}_{4+5}+M_{H,L})\not{\epsilon}^*\gamma_5\Gamma_c(Q^2)u_N}{\left[q_{4+5}^2-M_{H,L}^2-iM_{H,L}\Gamma_{H,L}\right]\left[q_{1-3}^2-M_{K^*}^2\right]},\\
i\mathcal{M}_d^{H,L} &= -\frac{ig'_{H,L}F_t^KF_{\rm EM}^{K\to K^*}\bar{u}_\Sigma(\not{q}_{4+5}+M_{H,L})(\epsilon^{\mu\nu\alpha\beta}k_{1\mu}\epsilon_\nu k_{3\alpha}\varepsilon^*_\beta)u_N}{\left[q_{4+5}^2-M_{H,L}^2-iM_{H,L}\Gamma_{H,L}\right]\left[q_{1-3}^2-M_K^2\right]},
\end{aligned}
\tag{2}
$$

where $q_{i\pm j} = k_i \pm k_j$. The polarization vectors for the incident photon and outgoing $K^*$ are denoted by $\epsilon_\mu$ and $\varepsilon_\mu$, respectively. We used the combined coupling constants $g_{H,L} = e_{K^*}g_{K^*N(H,L)}g_{\pi\Sigma(H,L)}$ and $g'_{H,L} = g_{\gamma KK^*}g_{KN(H,L)}g_{\pi\Sigma(H,L)}$ for convenience. The vertex functions $\Gamma_{a,b,c}$ are given by

$$
\begin{aligned}
\not{\Gamma}_a(Q^2) &= \not{\epsilon} + \left(F_1^p - 1\right)\left[\not{\epsilon} + \frac{(\epsilon\cdot k_1)\not{k}_1}{Q^2}\right] - \frac{\kappa_N F_2^p}{4M_N}(\not{k}_1\not{\epsilon} - \not{\epsilon}\not{k}_1),\\
\not{\Gamma}_b(Q^2) &= F_1^{H,L}\left[\not{\epsilon} + \frac{(\epsilon\cdot k_1)\not{k}_1}{Q^2}\right] - \frac{\kappa_{H,L}F_2^{H,L}}{4M_N}(\not{k}_1\not{\epsilon} - \not{\epsilon}\not{k}_1),\\
\Gamma_c(Q^2) &= \epsilon\cdot(2k_3-k_1) + (F^{K^*}-1)\left[\epsilon\cdot(2k_3-k_1) + \frac{(\epsilon\cdot k_1)[\epsilon\cdot(2k_3-k_1)]}{Q^2}\right].
\end{aligned}
\tag{3}
$$

The phenomenological prescription for the vertices in Eq. (3) satisfies the WTI for $Q^2 = 0$ [17,29] and $Q^2 \neq 0$ [6] simultaneously, and the invariant amplitudes defined in Eq. (2) can be also used similarly for the $\Lambda$ and $\Sigma$ BKG contributions by changing the baryon field $(H, L)$ into $\gamma_5 B$. Note that the invariant amplitude $\mathcal{M}_d$ is gauge invariant by itself because of the antisymmetric tensor-coupling structure.

In Eq. (2), we have introduced the strong $(F_x)$ and electromagnetic $(F_{\rm EM})$ form factors to reproduce experimental data, considering the internal structure of the hadrons. As for the strong form factors, the following parametrized form is employed:

$$
F_x = \frac{\Lambda_{\rm strong}^4}{\Lambda_{\rm strong}^4 + (x-M_x)^2}, \quad F_c = 1 - (1-F_s)\left(1-F_t^{K^*}\right).
\tag{4}
$$

Here, $\Lambda_{\rm strong}$ indicates the strong cutoff and the Mandelstam variables $x$ are defined as $s = (k_1+k_2)^2$, $t = (k_1-k_3)^2$, and $u = (k_2-k_3)^2$. Note that the invariant amplitudes $i\mathcal{M}_b$ and

TABLE II. The electric and magnetic mean-square charge radii for the high ($H$) and low ($L$) pole contributions (fm$^2$).

| $\langle r_E^2\rangle_H$ | $\langle r_M^2\rangle_H$ | $\langle r_E^2\rangle_L$ | $\langle r_M^2\rangle_L$ |
|---|---|---|---|
| $-0.131+0.303i$ | $0.267-0.407i$ | $0.018+0.002i$ | $-0.013+0.021i$ |

$i\mathcal{M}_d$ do not contain the common strong form factor $F_c$ because they are gauge invariant by themselves. $M_x$ stands for the mass of the propagating particles: $M_{s,t,u}=M_{K,K^*,Y}$. As for the $K$ exchange [Fig. 1(d)], we assign the strong form factor $F_t^K$ with $M_x=M_K$.

The Dirac ($F_1$) and Pauli ($F_2$) EM form factors for the proton read with its anomalous magnetic moment $\kappa_p=1.79$:

$$F_1^p(Q^2)=\frac{G_E^p(Q^2)+\tau G_M^p(Q^2)}{1+\tau},$$
$$F_2^p(Q^2)=\frac{G_M^p(Q^2)-G_E^p(Q^2)}{\kappa_B(1+\tau)},\quad \tau=\frac{Q^2}{4M_p^2}, \tag{5}$$

where the Sachs form factors are defined by [30]

$$G_E^p(Q^2)=G_D(Q^2),\quad G_M^p(Q^2)=(\kappa_B+1)G_D(Q^2),$$
$$G_D(Q^2)=\left(\frac{1}{1+Q^2/\Lambda_D^2}\right)^2,\quad \Lambda_D^2=0.71\,\mathrm{GeV}^2. \tag{6}$$

As for the neutral hyperons ($Y$) such as $\Lambda(1116)$, $\Sigma(1193)$, $H$, and $L$, we make use of the following form-factor parametrization, which was employed to reproduce the data for $\gamma^* p\to K^+\pi\Sigma$ [18]:

$$G_E^Y(Q^2)=-\frac{\langle r_E^2\rangle_Y}{6}Q^2F_K(Q^2)\left(\frac{1}{1+Q^2\langle r_M^2\rangle_Y/12}\right)^2G_D(Q^2),$$
$$G_M^Y(Q^2)=\mu\left(\frac{1}{1+Q^2\langle r_M^2\rangle_Y/12}\right)^2G_D(Q^2). \tag{7}$$

To obtain the Dirac and Pauli form factors for those hyperons, the following expressions are used:

$$F_1^Y(Q^2)=\frac{\left[G_E^Y(Q^2)+\tau G_M^Y(Q^2)\right]}{1+\tau},$$
$$F_2^Y(Q^2)=\frac{\left[G_M^Y(Q^2)-G_E^Y(Q^2)\right]}{\kappa_Y(1+\tau)}. \tag{8}$$

We emphasize that the Sachs form factors in this parametrization of Eq. (7) are defined with the electric and magnetic mean-square charge radii $\langle r_{E,M}^2\rangle_Y$. Although there are various theoretical estimations for $\Lambda(1116)$ and $\Sigma(1193)$, we use $\langle r_E^2\rangle=0.029\,\mathrm{fm}^2$ and $0.209\,\mathrm{fm}^2$, respectively, from the relativistic quark model [31], and the values of $\langle r_M^2\rangle$ are chosen to be zero for simplicity. We verified that the finite values of $\langle r_M^2\rangle$ do not make qualitative differences in the corresponding form factors as far as we resort to the parametrization in Eq. (7).

From the ChUM calculations [15], the values of $\langle r_{E,M}^2\rangle_{H,L}$ were estimated as listed in Table II and they will be used to obtain the EM form factors for $H$ and $L$. We note that the complex values of $\langle r_{E,M}^2\rangle_{H,L}$ will provide additional phase factors to the amplitude of electroproduction. The anomalous magnetic moments for the hyperons are chosen to be $\kappa_{\Lambda,\Sigma,H,L}=(-0.64, 0.72, 0.40, 0.30)$ from experiments and theories [15,27].

The charged vector-kaon EM form factor is parametrized with its mean-square charge radius by

$$F_{\mathrm{EM}}^{K^*}(Q^2)=\frac{1}{1+Q^2\langle r^2\rangle_{K^*}/6}, \tag{9}$$

and $\langle r^2\rangle_{K^*}=0.54\,\mathrm{fm}^2$, calculated from the Lorentz-covariant Dyson-Schwinger method [19]. As for the EM transition vertex with $K^*\to\gamma K$, $F_{\mathrm{EM}}^{K^*\to\gamma K}(Q^2)$ is necessary and defined by a simple flavor-SU(3)-symmetric extension of the result given in Ref. [20]:

$$F_{\mathrm{EM}}^{K^*\to\gamma K}(Q^2)=\frac{F_K}{3F_{K^*}}V(Q^2,M^2),$$
$$V(Q^2,M^2)\approx\int_0^1\frac{d\mathrm{u}}{\mathrm{u}}\phi_K(\mathrm{u})\exp\left[-\frac{Q^2(1-\mathrm{u})}{\mathrm{u}\Lambda^2}+\frac{m_{K^*}^2}{\Lambda^2}\right], \tag{10}$$

where $\phi_K(\mathrm{u})$ denotes the kaon light-cone wave function as a function of the longitudinal momentum fraction $\mathrm{u}=(0\sim1)$ for a quark inside the meson. The value of $\Lambda$ in Eq. (10) indicates the nonperturbative scale at which $\phi_K(\mathrm{u})$ is evaluated. In Refs. [21,22], the present authors employed the nonlocal chiral-quark model to compute $\phi_K(\mathrm{u})$, based on the instanton model, resulting in the following Gegenbauer polynomial expression:

$$\phi_K(\mathrm{u})\approx 6u(1-\mathrm{u})\left[1+3a_1^K(2\mathrm{u}-1)\right], \tag{11}$$

where the asymmetry coefficient turns out to be $a_1^K=0.06865$ at the energy scale of $\Lambda=1.2\,\mathrm{GeV}$ with the empirical values $f_{K,K^*}=(156.1, 204)\,\mathrm{MeV}$. Because we are also interested in the present reaction process in the low-energy region near the threshold, it must be consistent for us to use the above $\phi_K(u)$ for the transition form factor here. Using Eqs. (10) and (11), we introduce the following dipole-type parametrization, for numerical convenience,

$$F_{\mathrm{EM}}^{K^*\to\gamma K}(Q^2)=\left(\frac{\Lambda_{K^*\to\gamma K}^2}{\Lambda_{K^*\to\gamma K}^2+Q^2}\right)^2,\quad \Lambda_{K^*\to\gamma K}=1.1\,\mathrm{GeV}. \tag{12}$$

All the $Q^2$ dependence of the relevant EM form factors are plotted in Fig. 2. Note that we observe a tendency that $F_{\mathrm{EM}}^{K^*}\geqslant F_{\mathrm{EM}}^{K^*\to\gamma K}$ for all the $Q^2$ regions. In the numerical results, this tendency will play an important role in making the invariant-mass line shapes for the electroproduction with and without the $K^*N\Lambda^*$ interaction.

Although we have used the PS coupling scheme for the $PBB$ and $PB(H,L)$ Yukawa vertices, as shown in Eq. (1), there can be the pseudovector (PV) coupling:

$$\mathcal{L}_{PBB'}^{\mathrm{PV}}=-\frac{g_{PBB'}^{\mathrm{PV}}}{2f_\pi}\bar{B}'(\Gamma_5\partial\!\!\!/P)B+\mathrm{H.c.}, \tag{13}$$

where $\Gamma_5=(\gamma_5, 1_{4\times4})$ for the positive- or negative-parity $B$, whereas $B'$ is assumed to have positive parity. The PS and PV couplings satisfy the Goldberger-Treiman (GT)

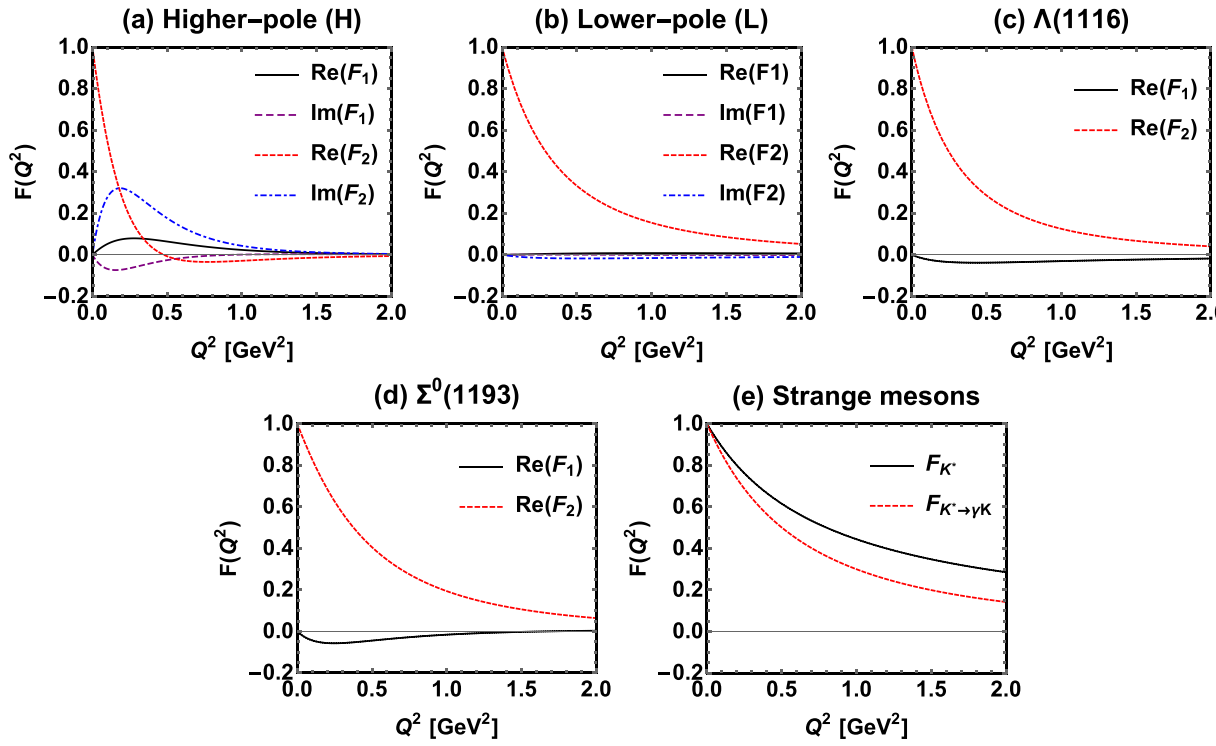


FIG. 2. EM form factors of various neutral hyperons (a)–(d) and strange mesons (e) as functions of $Q^2$ (GeV$^2$). The solid, dashed, dotted, and dot-dashed lines indicate Re$F_1$, Im$F_1$, Re$F_2$, and Im$F_2$, respectively. Here, $F_1$ and $F_2$ stand for the Dirac and Pauli form factors for spin-1/2 baryons.

relations [32] by

$$g^{\rm PV}_{PBB'} = \frac{2f_\pi g^{\rm PS}_{PBB'}}{|\Pi M + \Pi' M'|}, \tag{14}$$

where $\Pi$ and $M$ indicate the parity and mass of the corresponding baryon, respectively. In the PV scheme, we may have an additional term corresponding to the $\gamma PBB'$ contact interaction to preserve the WTI. However, in the present reaction process, the contact interaction disappears, because of the neutral pion electric charge. Using the PV Lagrangian and GT relation in Eqs. (13) and (14), the corresponding invariant amplitudes and coupling constants can be computed in a straightforward manner. However, we have verified that the PV scheme gives essentially the same results as the PS scheme by tuning the cutoff parameter for the form factors, defined in Eq. (4), by about 10%–15%. Hence, according to this observation, we will show the numerical results only from the PS scheme hereafter.

There are additional BKG contributions from the KR and WT interactions as shown in Figs. 1(e)–1(g) and their invariant amplitudes satisfying the WTI read

$$\begin{aligned}
i\mathcal{M}^{\rm KR}_e &= \frac{eG_{\rm KR}F_t^{K^*}F_{\rm EM}^{K^*}\bar{u}_\Sigma\gamma_5\not{\epsilon}^*(\not{q}_{1+2}+M_N)\not{V}_a(Q^2)u_N}{\left[q^2_{1+2}-M_N^2\right]},\\
i\mathcal{M}^{\rm KR}_f &= -\frac{eG_{\rm KR}F_t^{K^*}F_{\rm EM}^{K^*}\bar{u}_\Sigma\gamma_5\not{\epsilon}^*\Gamma_b(Q^2)u_N}{\left[q^2_{1-3}-M_{K^*}^2\right]},\\
i\mathcal{M}^{\rm WT}_g &= -\frac{ig_{\rm WT}g_{\gamma KK^*}F_t^K F^{K^*\to\gamma K}\bar{u}_\Sigma(\not{k}_1-\not{k}_3+\not{k}_4)(\epsilon^{\mu\nu\alpha\beta}k_{1\mu}\epsilon_\nu k_{3\alpha}\varepsilon^*_\beta)u_N}{\left[q^2_{1-3}-M_K^2\right]}.
\end{aligned} \tag{15}$$

We verify that these KR and WT contributions are numerically very tiny in comparison to the others because of the small values of $g_{\rm WT}$ and $G_{\rm KR}$ for $g = 1$–6.

The total amplitude for the present reaction process can be written with the resonance and BKG contributions as follows:

$$i\mathcal{M}_{\rm total} = \underbrace{e^{i\phi}(i\mathcal{M}_H + i\mathcal{M}_L)}_{\rm Resonance} + \underbrace{i\mathcal{M}_\Lambda + i\mathcal{M}_\Sigma + i\mathcal{M}_{\rm WT} + i\mathcal{M}_{\rm KR}}_{\rm BKG}. \tag{16}$$

TABLE III. Input values for the masses and full-decay widths for the higher- ($H$) and lower-pole ($L$) contributions from the ChUM calculation [2].

| $M_H$ | $\Gamma_H$ | $M_L$ | $\Gamma_L$ |
|---|---|---|---|
| 1430 MeV | 30 MeV | 1376 MeV | 126 MeV |

Note that the phase factor between the $\Lambda$ and $\Sigma$ contributions is determined by the Nijmegen potential model. Although there can be certain phase factors between the hyperon contributions and the (KR, WT) ones, we ignore them, by taking into account the numerical results showing $|i\mathcal{M}_{\Lambda,\Sigma}| \gg |i\mathcal{M}_{\mathrm{WT,KR}}|$. However, because the strengths of the resonance contributions are compatible with those of the hyperon BKG ones, we introduce a phase factor $e^{i\phi}$ between them, whereas the phase between the $H$ and $L$ contributions are determined by ChUM. The phase angle $\phi$ will be treated as a free parameter ($0 \leqslant \phi \leqslant \pi$).

## III. NUMERICAL RESULTS AND DISCUSSIONS

In this section, we demonstrate the numerical results with relevant discussions in detail. The input values for the masses and full decay widths for ($H, L$) are listed in Table III, based on the ChUM results [16]. We note that the masses and full-decay widths for the higher- ($H$) and lower-pole ($L$) contributions depend on the regularization schemes in general in ChUM [33], providing about a few percent differences. However, those differences do not make any considerable changes in our conclusion of the present work.

First, we show the numerical results for the invariant-mass line shapes as functions of $M_{\pi^0\Sigma^0} \equiv M_I$, i.e., $d\sigma/dM_I$, for each contribution ($H$, $L$, $\Lambda$, $\Sigma$, WT, and KR) for $Q^2 = 0$ (photoproduction) and $Q^2 = 2\,\mathrm{GeV}^2$ (electroproduction) in Figs. 3(a) and 3(b), respectively. Here, we choose $\sqrt{s} = 2.35\,\mathrm{GeV}$ and the strong cutoff parameter for Eq. (4) is set to be 0.9 GeV, which was employed to reproduce the experimental data for $\gamma p \to K^+\Lambda(1405)$ [6], because we have not had experimental data for the $K^*$ production to compare with the theory at this moment. Note that the order of the cross sections for the electroproduction is much smaller than those for the photoproduction, because of the EM form factors as shown in Fig. 2.

For the photoproduction and electroproductions, respectively, we observe the strongly destructive and slightly constructive interferences between the $\Lambda$ and $\Sigma$ BKG contributions. The different interference pattern can be understood by additional phase factors in the electroproductions as shown in Fig. 1(b) and the EM form factors in Fig. 2. On the contrary, we find that the WT contribution is relatively small and the KR one almost negligible for $g = 1$. Thus, these $\Lambda$ and $\Sigma$ BKG contribution make almost all the strengths of the nonresonant BKG contributions. It also turns out that the EM form factors for the electroproduction make the BKG strength much smaller by a factor $\sim 10^{-2}$ and the BKG shape tilted to the lower $M_I$ region in comparison to the photoproduction, because of the interference pattern changes by the EM form factors as mentioned.

In Fig. 3, we show various contributions to the $\pi^0\Sigma^0$ invariant-mass distributions (line shape). It turns out that the lower-pole ($L$) contribution is almost negligible in comparison to the higher-pole ($H$) one for the photoproduction and electroproductions because of the much wider decay width of the lower-pole contribution as listed in Table III. Although the lower-pole contribution couples strongly to the $\pi\Sigma$ channel as mentioned previously in Sec. I, $|g_{K^*NH}|$ is about two times larger than $|g_{K^*NL}|$ as shown in Table I. As a result, it turns out that the reduced coupling constants exhibit $|g_{K^*NH}g_{\pi\Sigma H}| \approx |g_{K^*NL}g_{\pi\Sigma L}|$. Therefore, the strength difference between the higher- and lower-pole contributions becomes more significant in the $K^*\pi\Sigma$ channel in comparison to the $K\pi\Sigma$ channel, which shows $|g_{KNH}g_{\pi\Sigma H}| < |g_{KNL}g_{\pi\Sigma L}|$.

If the $K^*N\Lambda^*$ interaction is absent ($g = 0$), the $K$ exchange dominates the reaction process and the $H$ peaks show small but finite strengths in comparison to the BKG contributions. When the $K^*N\Lambda^*$ interaction turns on with $g = 1$, the situation changes drastically. As for the photoproduction, the effects of the inclusion of the $K^*$ exchange gives about 0.1 $\mu$b increase in the $H$ peak position because of a constructive interference between the $K$ and $K^*$ exchanges. The increase

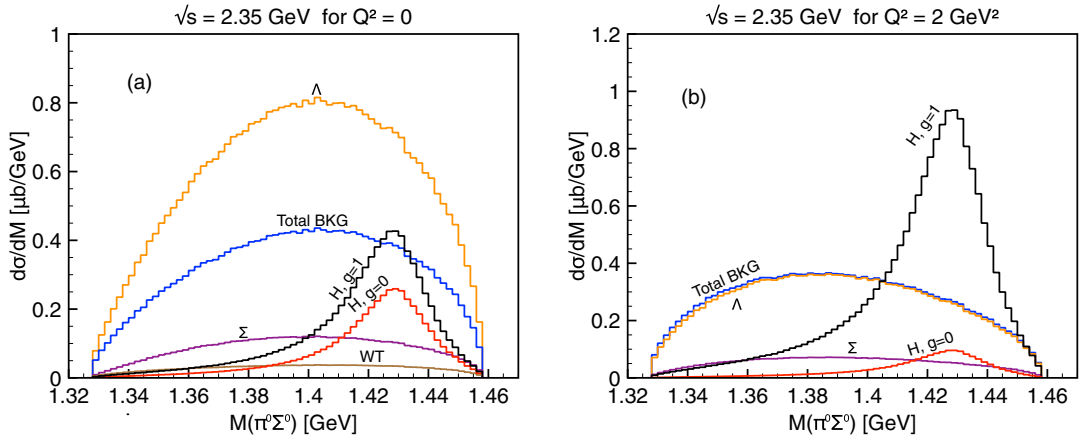


FIG. 3. Each contribution for $\pi^0\Sigma^0$-invariant-mass line shape ($d\sigma/dM_{\pi^0\Sigma^0}$) for (a) $Q^2 = 0$ and (b) $Q^2 = 2\,\mathrm{GeV}^2$ at $\sqrt{s} = 2.35\,\mathrm{GeV}$.

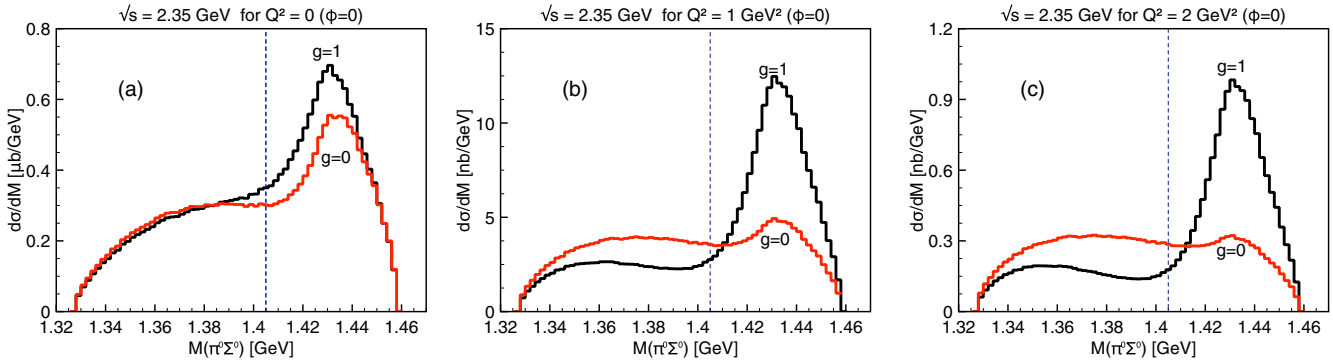


FIG. 4. $\pi^0\Sigma^0$ invariant-mass plot ($d\sigma/dM_{\pi^0\Sigma^0}$) for (a) $Q^2 = 0$, (b) $Q^2 = 1.0\,\mathrm{GeV}^2$, and (c) $Q^2 = 2.0\,\mathrm{GeV}^2$ at $\sqrt{s} = 2.35\,\mathrm{GeV}$ for $\phi = 0$, using different choices of the parameter $g = 1$ and 0, which correspond to the cases with and without the $K^*$-exchange contribution in the $t$ channel. The vertical dashed line corresponds to the mass of $\Lambda(1405)$. See the text for the details.

from the $K^*$ exchange is more pronounced for the electroproduction because the $K^*$ EM form factor is larger than that of the $K^* \to \gamma K$ transition one at $Q^2 = 2\,\mathrm{GeV}^2$ as shown in Fig. 2, resulting in the clearer peak signal at $M_I = 1.43\,\mathrm{GeV}$ over the BKG, as shown in Fig. 3(b).

Now, we present the numerical results for the invariant-mass line shape including all the contributions, varying the phase angle $\phi$ defined in Eq. (16) as a free parameter. For simplicity, we only consider two cases with $\phi = 0$ and $\pi$, and those results are shown in Fig. 4 and Fig. 5, respectively. The vertical dashed line indicates $M_I = 1.405\,\mathrm{GeV}$. As for the case with $\phi = 0$ and $Q^2 = 0$ (photoproduction) shown in Fig. 4(a), it turns out that the $H$ and BKG contributions interfere constructively, showing a very pronounced peak in the vicinity of $M_I = 1.43\,\mathrm{GeV}$, and a broad bump for $M_I \lesssim 1.4\,\mathrm{GeV}$ because of the BKG contributions. Again, we observe that the inclusion of the $K^*$ exchange gives small increases in the peak region, but the line shape remains almost the same.

As for the electroproduction for $Q^2 = (1, 2)\,\mathrm{GeV}^2$ in Figs. 4(b) and 4(c), the $H$ peak becomes enhanced considerably, according to the larger $K^* \to \gamma K$ transition form factor than the $K^*$ EM one as explained previously. From these numerical results, we conclude that the $\Lambda^*$ peak can be clearly observed both for the photoproduction and electroproductions, if the $K^*N\Lambda^*$ interaction is finite. On the contrary, if the interaction is negligible, the clear peak signal survives only for the photoproduction. Hence, the electroproduction is better to test the effects of the $K^*N\Lambda^*$ interaction. In Fig. 5, we also draw the same curves for $\phi = \pi$ and observe similar tendencies, although the $H$ and the BKG contributions interfere destructively. It turns out that this destructive interference makes the $H$ peak more dubious for $g = 0$ than that with $\phi = 0$. In general, the peak signal decreases with respect to $Q^2$.

Finally, we are in a position to define a polarization observable as a function of $M_I$, which is similar to the photon-beam asymmetry, and responsible for estimating the effects of the $K^*$-exchange contribution:

$$\Sigma(M_I) = \frac{d\sigma_x/dM_I - d\sigma_y/dM_I - d\sigma_z/dM_I}{d\sigma_x/dM_I + d\sigma_y/dM_I + d\sigma_z/dM_I}, \tag{17}$$

where the subscripts $x$, $y$, and $z$ denote the photon linear polarizations $\vec{\varepsilon}_x$ (perpendicular), $\vec{\varepsilon}_y$ (parallel), and $\vec{\varepsilon}_z$ (longitudinal). Here, the incident photon and outgoing $K^*$ determines the $y$-$z$ reaction plane in the center-of-mass frame, as shown in Fig. 6(a). Note that the third term $d\sigma_z/dM_I$ in Eq. (17) only exists for the electroproduction. In Fig. 6(b), we depict the numerical results of $\Sigma$ for the photoproduction ($Q^2 = 0$), using various choices of the model parameters. The shaded area represents the $H$ peak region.

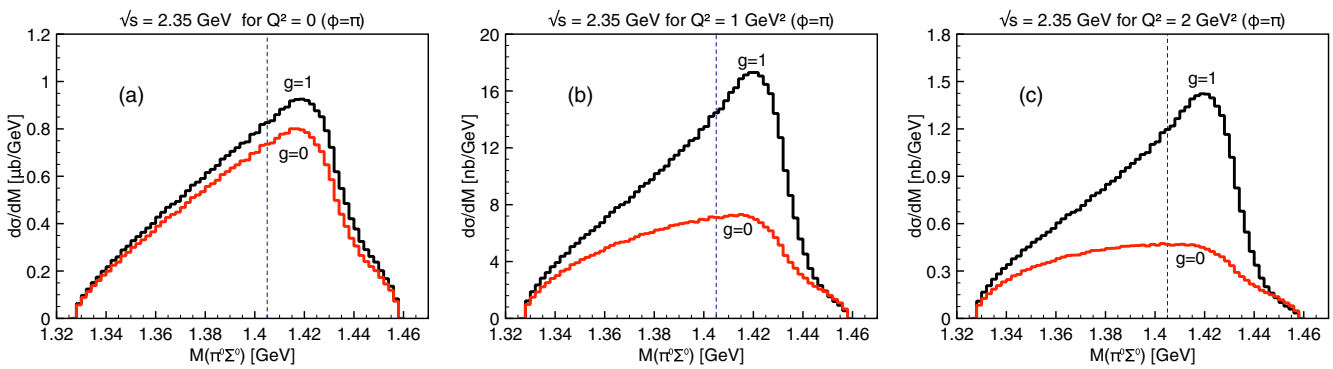


FIG. 5. $\pi^0\Sigma^0$-invariant-mass plots in the same manner as in Fig. 4 for $\phi = \pi$. See the text for the details.

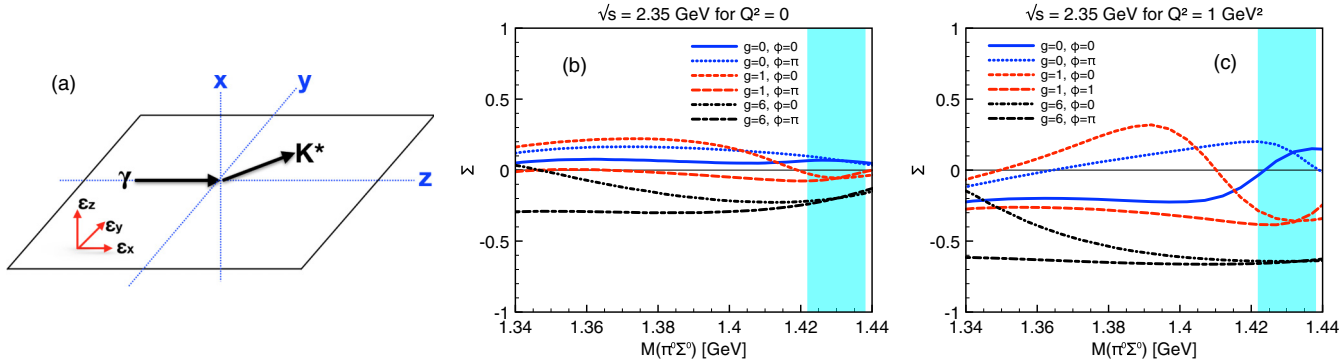


FIG. 6. (a) Definition for the photon polarizations and the relevant momenta for $\Sigma$, defined in Eq. (17). (b) Numerical results for $\Sigma$ with $Q^2 = 0$ varying $g$ and $\phi$. The vertical shaded area represents the higher-pole peak region. (c) The same with $Q^2 = 1\,\mathrm{GeV}^2$.

As for $g = 0$, i.e., the reaction process is dominated by the $K$-exchange and the values of $\Sigma$ are *positive*. This observation indicates that the $K$-exchange contribution almost disappears for the parallel polarization $d\sigma_y/dM_I \sim 0$ because of the antisymmetric-tensor structure of $\mathcal{M}_d$ in Eq. (2) $\propto \vec{\epsilon}_\gamma \times \vec{k}_{K^*}$. In contrast, if we take into account the $K^*$-exchange contribution with $g = 1$, the perpendicular contribution $d\sigma_x/dM_I$ becomes negligible, resulting in the negative $\Sigma$ values in the peak region as shown in Fig. 6(a). Again, this behavior can be explained by the Lorentz structure of $\mathcal{M}_{a,b,c}$ in Eq. (2) $\propto \vec{\epsilon}_\gamma \cdot \vec{k}_{K^*}$. As shown by the curves for $g = 6$, this tendency becomes more apparent because the higher-pole contribution dominates the cross section for the larger $g$ values.

In Fig. 6(c), we show the numerical results of $\Sigma$ for the electroproduction in the same manner as the photoproduction. Because the spin-0 scalar component of the longitudinal photon polarization enhances the spin-1 exchange contribution, i.e., the $K^*$-exchange one, the third term in Eq. (17) is magnified. Hence, as shown in Fig. 6(c), the signals in the peak regions become more obvious for $g = 1$. Note that we observe the same tendency with respect to the larger $g$ for the electroproduction as well.

Taking these numerical results of $\Sigma$ into account, if one observes the positive $\Sigma$ values for the photoproduction and electroproductions in the vicinity of the peak region in experiments, it indicates the $K^*$-exchange contribution must be negligible. In contrast, one can conclude that $K^*N\Lambda^*$ interaction is sizable, when the negative values of $\Sigma$ are measured. Consequently, by examining the sign of $\Sigma$ in the peak region experimentally, one can estimate the strength of $g_{K^*N\Lambda^*}$ uniquely.

## IV. SUMMARY

In the present work, we investigated the $K^*$ photoproduction and electroproductions via $\gamma^* p \to K^{*+}\pi^0\Sigma^0$, in which $\Lambda(1405) \equiv \Lambda^*$ appears as a dominant hyperon resonance near the threshold. Moreover, this reaction process does not contain $\Sigma^*(1385)$, which can interfere with $\Lambda^*$ in the charged channels such as $\gamma^* p \to K^{*+}\pi^\mp\Sigma^\pm$, resulting in a clear signal only from $\Lambda^*$. The effective Lagrangian method was employed at the tree-level Born approximation. We used the phenomenological strong and electromagnetic (EM) form factors for the relevant hadrons, and the EM form factors for $\Lambda^*$ was parametrized by using the information from the ChUM results. The $K^* \to \gamma K$ transition form factor was devised from the kaon light-front wave function, which was computed by the nonlocal chiral-quark model in our previous works, whereas the proton and vector kaon EM form factors were taken from available data. Focusing on the two-pole structure scenario of $\Lambda^*$ and the rarely known $K^*N\Lambda^*$ coupling constant $g_{K^*N\Lambda^*}$, we provide the numerical results for the invariant-mass line shape and the photon linear-polarization observable $\Sigma$. We list important observations in the present work as follows:

The lower-pole peak ($L$) turns out to be unseen because of its larger width $\Gamma_L \approx 126\,\mathrm{MeV} \gg \Gamma_H \approx 30\,\mathrm{MeV}$, when we resort to the ChUM results as theory inputs. It also turns out that the background (BKG) contribution comes mainly from the destructive and constructive interferences between $\Lambda$ and $\Sigma$ ground states for the photoproduction and electroproduction, respectively. This different interference pattern can be understood by their EM form factors, which modify the phases between the invariant amplitudes.

We find that the $\Lambda^*$ peak is clearly observed for the photoproduction and electroproductions with the finite $K^*N\Lambda^*$ interaction, whereas the peak survives only for the photoproduction when we ignore the interaction. These interesting behaviors of the peak can be understood by the different $Q^2$ dependencies in the $K^*$ electromagnetic and $K^* \to \gamma K$ transition form factors. Taking into account these observations, if the line shapes of the photoproduction and electroproduction exhibit considerable differences in the peak region, it can be said that the $K^*NH$ interaction is not important.

To estimate the strength of the $K^*N\Lambda^*$ interaction more precisely, we suggest a photon-polarization observable $\Sigma$. As for the photoproduction, where the longitudinal polarization does not exist, the $K$- and $K^*$-exchange contributions are almost canceled out for the parallel and perpendicular polarizations, respectively. Hence, by construction, $\Sigma$ becomes positive and negative in the peak region $M_I \sim 1.43\,\mathrm{GeV}$ for the finite and negligible $K^*NH$ interaction, respectively. When the longitudinal

photon polarization, which gives the spin-0 scalar (natural spin-parity) component, comes into play for the electroproduction, it enhances the $K^*$-exchange contribution and the negative signal becomes more obvious. Thus, by examining the polarization observable $\Sigma$ in the vicinity of the $H$ peak, one can estimate the strength of $g_{K^*NH}$ in the experiments.

Although there are several theoretical uncertainties, such as the parametrization of the relevant form factors, we have provided theoretical results for understanding the nature of $\Lambda^*$ produced with the vector kaon and also suggested how to estimate the $K^*N\Lambda^*$ interaction strength uniquely for the future experiments by the LEPS and CLAS collaborations. More realistic production processes including the decay of $K^* \to \pi K$ in the four-body phase space and the $\Lambda^*$ production with the pseudoscalar-meson beam, such as $\pi N \to K\pi\Sigma$, are being studied, and the related works will appear elsewhere.

## ACKNOWLEDGMENTS

The authors thank K. P. Khemchandani, A. Martinez Torres, and J. K. Ahn for fruitful discussions. The work of S.i.N. was supported by the National Research Foundation of Korea (NRF) (Grants No. 2018R1A5A1025563 and No. 2019R1A2C1005697). The work of A.H. is supported in part by the Grants-in-Aid for Scientific Research [Grant No. JP17K05441 (C)].

[1] H. Leutwyler, Ann. Phys. **235**, 165 (1994).
[2] D. Jido, J. A. Oller, E. Oset, A. Ramos, and U. G. Meissner, Nucl. Phys. A **725**, 181 (2003).
[3] V. K. Magas, E. Oset, and A. Ramos, Phys. Rev. Lett. **95**, 052301 (2005).
[4] D. Jido, E. Oset, and A. Ramos, Phys. Rev. C **66**, 055203 (2002).
[5] T. Hyodo and D. Jido, Prog. Part. Nucl. Phys. **67**, 55 (2012).
[6] S. i. Nam, Phys. Rev. D **96**, 076021 (2017).
[7] L. Roca and E. Oset, Phys. Rev. C **87**, 055201 (2013).
[8] L. Roca and E. Oset, Phys. Rev. C **88**, 055206 (2013).
[9] J. M. M. Hall, W. Kamleh, D. B. Leinweber, B. J. Menadue, B. J. Owen, A. W. Thomas, and R. D. Young, Phys. Rev. Lett. **114**, 132002 (2015).
[10] A. Cieplý, M. Mai, U. G. Meissner, and J. Smejkal, Nucl. Phys. A **954**, 17 (2016).
[11] H. Y. Lu *et al.* (CLAS Collaboration), Phys. Rev. C **88**, 045202 (2013).
[12] M. Niiyama (LEPS TPC Collaboration), Nucl. Phys. A **827**, 261C (2009).
[13] K. Moriya *et al.* (CLAS Collaboration), Phys. Rev. C **88**, 045201 (2013); **88**, 049902 (2013).
[14] K. Moriya *et al.* (CLAS Collaboration), Phys. Rev. C **87**, 035206 (2013).
[15] T. Sekihara, T. Hyodo, and D. Jido, Phys. Lett. B **669**, 133 (2008).
[16] K. P. Khemchandani, A. Martinez Torres, H. Kaneko, H. Nagahiro, and A. Hosaka, Phys. Rev. D **84**, 094018 (2011).
[17] S. i. Nam, J. Phys. G **40**, 115001 (2013).
[18] M. M. Kaskulov and P. Grabmayr, Eur. Phys. J. A **19**, 157 (2004).
[19] F. T. Hawes and M. A. Pichowsky, Phys. Rev. C **59**, 1743 (1999).
[20] A. Khodjamirian, Eur. Phys. J. C **6**, 477 (1999).
[21] S.-i. Nam, H.-C. Kim, A. Hosaka, and M. M. Musakhanov, Phys. Rev. D **74**, 014019 (2006).
[22] S.-i. Nam and H.-C. Kim, Phys. Rev. D **74**, 076005 (2006).
[23] D. Keller *et al.* (CLAS Collaboration), Phys. Rev. D **83**, 072004 (2011).
[24] R. Dhir and R. C. Verma, Eur. Phys. J. A **42**, 243 (2009).
[25] A. C. Wang, W. L. Wang, F. Huang, H. Haberzettl, and K. Nakayama, Phys. Rev. C **96**, 035206 (2017).
[26] S. Y. Ryu *et al.* (LEPS Collaboration), Phys. Rev. Lett. **116**, 232001 (2016).
[27] C. Patrignani *et al.* (Particle Data Group), Chin. Phys. C **40**, 100001 (2016).
[28] V. G. J. Stoks and T. A. Rijken, Phys. Rev. C **59**, 3009 (1999).
[29] R. M. Davidson and R. Workman, Phys. Rev. C **63**, 025210 (2001).
[30] C. F. Perdrisat, V. Punjabi, and M. Vanderhaeghen, Prog. Part. Nucl. Phys. **59**, 694 (2007).
[31] K. Berger, R. F. Wagenbrunn, and W. Plessas, Phys. Rev. D **70**, 094027 (2004).
[32] S. i. Nam, A. Hosaka and H. C. Kim, Phys. Lett. B **579**, 43 (2004).
[33] S.-i. Nam, H.-C. Kim, T. Hyodo, D. Jido, and A. Hosaka, J. Korean Phys. Soc. **45**, 1466 (2004).